Spreading dynamics of terraced droplets

Santiago Betelú,[1] Bruce M. Law,[1] and C. C. Huang[2]
[1]*Condensed Matter Laboratory, Department of Physics, Kansas State University, Manhattan, Kansas 66506-2601*
[2]*Department of Physics, University of Minnesota, Minneapolis, Minnesota 55455*
(Received 6 August 1998)

The liquid crystal $\overline{7}S5$ spreads as a two-terraced droplet on an oxide covered (100) Si wafer. The thickness of the upper and lower terraces are respectively ~ 200 and ~ 40 Å. This is the simplest system for which the de Gennes and Cazabat (dGC) terraced spreading model [C. R. Acad. Sci. II **310**, 1601 (1990)] is applicable. We find that soon after the upper terrace acquires a flat top a hole develops in the center of this terrace. The hole propagates down to the depth of the first terrace. In this contribution we demonstrate that the dGC model is unstable to the formation of a hole in the center of the upper terrace for a two-terraced droplet. Our extended dGC model, which includes a hole in the upper terrace, provides a reasonable description of the *average* spreading dynamics for this system. However, this model has difficulties quantitatively accounting for all of the features exhibited by the dynamics, perhaps because experimentally the inner and outer borders of the upper terrace become irregular with time. These irregularities in the borders have not been included within the model. [S1063-651X(99)04006-4]

PACS number(s): 68.10.Gw, 68.15.+e, 61.30.−v, 68.45.−v

I. INTRODUCTION

The spreading of liquid droplets is very important for an understanding of lubrication, molecular scale friction, and coating dynamics [1,2]. One of the most interesting features observed in the spreading of nonvolatile liquid droplets on completely wettable surfaces is the formation of molecular size terraces which precede the spreading of the macroscopic droplet across the surface. These first few molecular layers are frequently called precursor layers. The existence of precursor films has been known since early in the century [3] but only recently have sufficiently sensitive experimental techniques been used to quantify their existence. The precursor film can take a number of different forms. It can either vary continuously from a molecular size at the precursor film tip to a mesoscopic or macroscopic size at the droplet center [4] or it can consist of one or more terraced layers at the edge of the mesoscopic or macroscopic droplet [5]. When terracing is present the droplet may acquire the shape of a very flat pyramid. Cazabat and co-workers [6] provide a fascinating catalog of the many diverse forms that a spreading ''pyramid-shaped'' droplet can take under differing conditions. The reasons for the differing shapes of the precursor film are not completely understood at this time, however, it is believed to depend upon many different factors such as the atomic scale friction, the long and short-range interactions between the fluid molecules and the substrate, smectic layering induced by the presence of a hard boundary, and the presence of any adsorbed water molecules. These experimental studies have stimulated numerous theoretical investigations [7,8] and computer simulations [9], however, this field is far from understood either theoretically or experimentally.

In Ref. [7] de Gennes and Cazabat (dGC) have developed a conceptually simple model of terraced spreading when many terraces can be present. They assume that terracing exists and then determine the motion caused by the permeation of molecules from an upper terrace to a lower terrace assuming that the fluid at each terrace is incompressible. The motion is somewhat complicated because the motion of one terrace is coupled to the motion of other terraces. Cazabat and co-workers [5] have observed terraced droplets in many different types of systems, however, the terraces that she and co-workers have observed frequently have rounded edges (with rounding $\sim 0.1-0.5$ mm [10]) or alternatively possess sloping terraces [11] or a rounded droplet on top of the upper terrace. These terraced droplets therefore do not conform precisely to the situation studied theoretically by dGC where they assume flat terraces with sharp edges between terraces (Fig. 1). A more ideal terraced droplet was observed by Daillant, Zalczer, and Benattar [12] for the liquid crystal 8CB spreading on a (400) silicon wafer where three terraces with flat tops and sharp edges were observed. Curiously near the

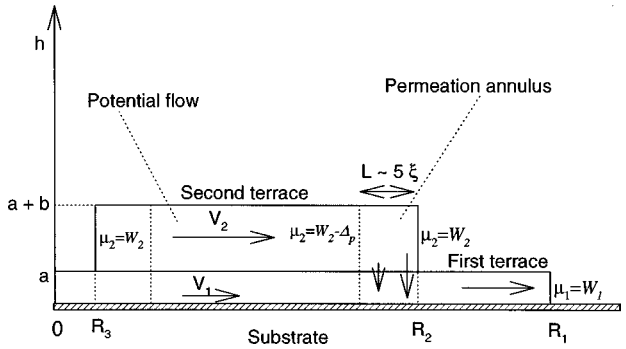

FIG. 1. Sketch of a two-terraced droplet as a function of radial distance r from the center of the drop. The first and second terraces, respectively, possess a thickness of a and b. The second terrace has an inner border (or hole) at R_3 and outer border at R_2, while the first terrace has a border at R_1. The chemical potential at each of these free borders is $\mu_i = W_i$. Permeation from the second terrace to the first terrace is much greater near R_2 than near R_3. The permeation near R_2 causes a drop in chemical potential at $r = R_2 - L$ of $\mu_2 = W_2 - \Delta_p$, which drives the flow in the second terrace and increases the size of the hole at R_3. Our model is restricted to the case where the permeation length $\xi \ll R_i$ and $\xi \ll R_2 - R_3$.

later part of the spreading dynamics, when only two terraces remained, holes were observed to form in the upper terrace. Daillant, Zalczer, and Benattar did not study the hole dynamics in detail nor did they provide an explanation for the growth of holes.

The ideal system to apply the dGC model to is one which consists of terraces possessing both perfectly flat tops and a sharp edge between terraces. In this paper we describe the spreading dynamics of such a system. The spreading dynamics of the liquid crystal 4-*n*-pentylphenyl-4′-*n*-heptyloxythiobenzoate ($\overline{7}S5$) on an oxide covered (100) silicon wafer, at the later stages, consists of only two terraces which possess flat tops and sharp edges between terraces (that is edges which are sharper than our spatial resolution of ~ 10 μm). As in Ref. [12] we find that this two terraced droplet spreads via the formation of a hole, that in our case, is at the center of the second terrace.

In this paper we are primary interested in the final stages of terraced spreading when only two terraces exist with a hole at the center of the upper terrace. The scope of this paper is not to explain the terraced structure or the nucleation of the hole, rather our purpose is to use a simple heuristic model, specifically the dGC model, to describe the average spreading dynamics without taking into account the detailed internal structure of the liquid crystal. In this model terraces of constant thickness are assumed to be present. We extend this model to include a hole at the center of a two-terraced droplet; surprisingly, despite the simplicity of this model a reasonable qualitative description of the spreading dynamics for the liquid crystal $\overline{7}S5$ is obtained.

II. EXPERIMENTS

The (100) silicon wafer substrates that we use were purchased from Semiconductor Processing Company. They are polished on one side and possess *n*-type phosphorus doping, a resistivity of $1-10$ Ω cm and dimensions of $3.8\times 3.8\times 0.32$ cm^3. The surface is typically covered by a uniform oxide layer of thickness ~ 20 Å. The silicon wafers go through a rigorous cleaning procedure before use. They are first cleaned with an ''organic mixture'' consisting of a solution of $H_2O+H_2O_2+NH_4OH$ in the ratio 6:1.5:1 for 15 min at 75 °C followed by cleaning in a ''metallic mixture'' consisting of $H_2O+H_2O_2+HCl$ in the ratio 7.5:1.5:1 for 15 min at 75 °C. These two cleaning procedures remove, respectively, most trace organic and metallic impurities from the surface [13]. The wafer is finally rinsed in distilled deionized water and then vapor degreased in isopropyl alcohol [14]. Isopropyl alcohol and water are completely miscible so that any residual water on the wafer surface is removed and the substrate can be readily dried in an oven at 110 °C without any observable ''water stains.'' Just prior to usage the wafers are uv ozone cleaned [15] for one hour to ensure the absence of organic contaminants. After this procedure, complete wetting with water is achieved as an indication of the excellent quality of the cleaning procedure.

The liquid crystal $\overline{7}S5$, used in the experiments, possesses an interesting phase diagram [16]. On heating $\overline{7}S5$ melts at 53.5 °C and exhibits an isotropic-nematic phase transition at 82.1 °C on both heating and cooling. For bulk samples this system can be supercooled to well below its melting point. A nematic-smectic transition is observed at 37.0 °C while the system recrystallizes at 23 °C.

In our experiments a small crystal of $\overline{7}S5$ is deposited on a clean Si wafer at room temperature using a glass micromanipulator and an optical microscope. The volume V of these crystals varied between 10 and 60 pl. The Si wafer and liquid crystal were then placed inside a closed oven which was rapidly heated to 55 °C. At this temperature the liquid crystal melts and spreads on the Si wafer surface as two well defined terraces. The spreading dynamics are studied inside this oven, where the temperature variations are below 0.002 °C, and the silicon wafer is situated on a solid copper block in order to minimize thermal gradients. Images of the drop are obtained with an ellipsometric microscope [17,18] whose angle of incidence is fixed at the Brewster angle for the oxide covered Si wafer ($\theta_B=75.5°$). Imaging optics provide a spatial resolution of better than 10 μm$\times$40 μm while the vertical film thickness resolution is 1 Å. The acquisition of each image into a personal computer takes only a few seconds. This time is short compared with the spreading time of typically a couple of hours. The ellipsometric signal obtained by the microscope $\mathrm{Im}(r_p/r_s)$, where r_p and r_s are, respectively, the effective complex reflection amplitudes for the p and s polarizations, is converted to thickness h as a function of position on the Si wafer substrate [19] by modeling each point on the droplet as a homogeneous isotropic dielectric layer possessing an average refractive index of $n=1.5$ [20].

III. EXPERIMENTAL RESULTS

The spreading of the droplets progresses through a number of differing stages.

(1) In the first stage the droplet height profile $h(r)$, as a function of the radial distance r from the center of the droplet, possesses a rounded shape similar to capillarity dominated spreading of any ordinary liquid. An extraordinary feature of the droplet, at this stage, is the shape of the droplet border with the wafer; at the droplet border the thickness decreases ''precipitously'' to the wafer value over a height of ~ 250 Å in less than our spatial resolution of 10 μm.

(2) Next a precursor film of thickness $a\approx 40$ Å appears at the border of the drop while the central part of the drop still remains rounded [Fig. 2(a), curve *A*]. Throughout the spreading process the thickness of this precursor film is constant within our experimental resolution of 1 Å [21]. The time when the precursor film first appears will be denoted by t_0.

(3) With increasing time the central part of the drop becomes progressively flatter and its maximum height h_2 approaches an asymptotic value of $h_f=a+b$ in an approximate exponential fashion [Fig. 3(a)], where b is the thickness of the second terrace. When the height reaches this asymptotic value, the central portion of the upper terrace is flat. It is at this stage that a hole first appears at the center of the second terrace [Fig. 2(a), curve *B*]. This hole rapidly propagates down to the depth of the first terrace [Fig. 2(a), curve *C*]. The hole is initially quite circular however with increasing time the inner and outer edges of the second terrace are progressively ''eaten'' away and the borders may become irregular [Fig. 2(b)]. Note that the thickness of the first and second

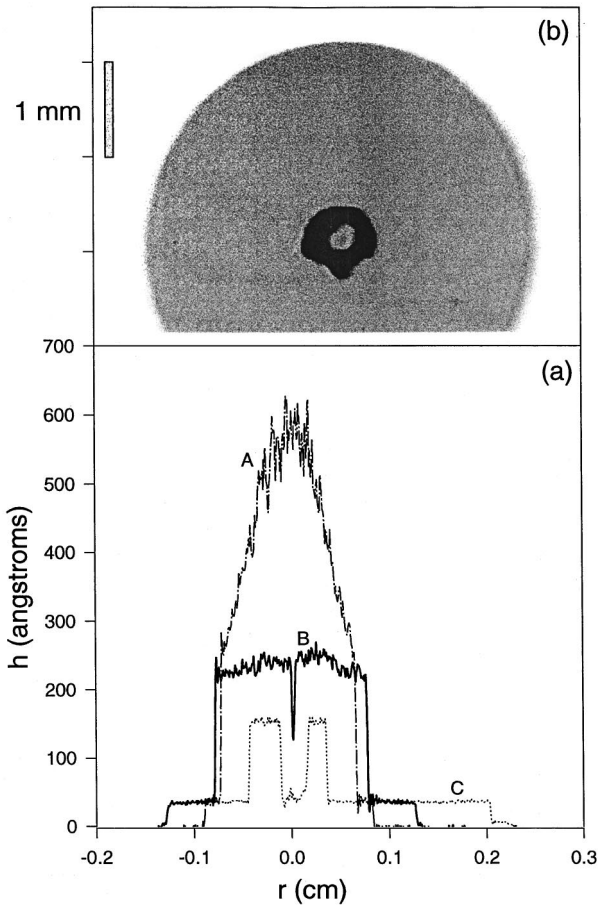

FIG. 2. (a) Height profile $h(r)$ for the liquid crystal $\overline{7}S5$ of volume 60.5 pl spreading on a (100) Si wafer surface at different normalized times $T=(t-t_0)/(t_f-t_0)$, $T=0.01$ (*A*), 0.10 (*B*), and 0.77 (*C*) where t_0 and t_f represent, respectively, the time when the precursor layer first appears and the time when spreading stops. In B the hole of radius R_3 is just starting to form. For curve *C* the hole has propagated to the depth of the first terrace, and the second terrace is extremely flat on top with a sharp outer border of radius R_2. (b) Two-dimensional image of the spreading droplet of curve *C*, where the profile in (a) is a vertical cut through the center of droplet. The gray bar corresponds to a length scale of 1 mm.

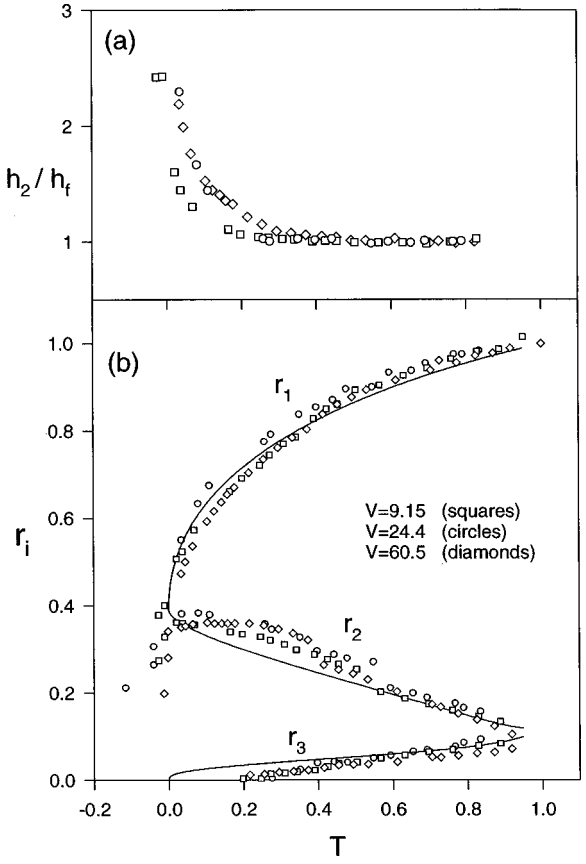

FIG. 3. (a) Relative height (h_2/h_f) of the second terrace as a function of the normalized time (T), where $h_f=a+b$ is the asymptotic height. The extended dGC model is expected to be most accurate for h_2 constant, namely, for $T>0.2$. (b) Experimental time evolution (symbols) of the average, normalized radius of the precursor (r_1), second terrace (r_2), and hole (r_3) for droplet volumes of 9.15, 24.4, and 60.5 pl, where $r_i=R_i/R_f$ and R_f is the asymptotic radius of the first terrace. The solid line represents a fit to the extended dGC model [Eqs. (26)–(29)] with $\xi/R_f=0.0025$ for fixed $b/a=5.5$.

terraces, *a* and *b*, respectively, remain *constant* throughout this later stage when a hole is present.

(4) Finally, the spreading stops when the second terrace disappears at time t_f. The surface is then covered by a circular static layer of thickness *a*.

It is convenient to measure events in terms of the normalized time $T=(t-t_0)/t_l$ where t is time and $t_l=t_f-t_0$ is the ''lifetime'' of the droplet measured from when the precursor film first appears at time t_0 until the time when the second terrace disappears at t_f. In terms of this normalized time the first terrace appears at $T=0$, the hole in the second terrace appears approximately when the height of the second terrace becomes time independent at $T\simeq 0.2$ [Fig. 3(a)], while the spreading process finishes at $T=1$.

In Fig. 3(a) we have plotted the maximum height of the droplet h_2 divided by its asymptotic value $h_f=a+b$ as a function of the normalized time *T* defined above. In Fig. 3(b) we show the time evolution of the average reduced radii $r_i=R_i/R_f$ for the first terrace r_1, the second terrace r_2, and for the hole r_3, for three different volumes as a function of *T*. Here the radii have been divided by the final radius $R_f=\sqrt{V/\pi a}$ of the monolayer. For all of the data sets representing three different droplet sizes the relative height h_2/h_f [Fig. 3(a)] and the reduced radii r_i [Fig. 3(b)] fall on an approximate universal curve when plotted as a function of the normalized time *T*. This universality holds despite the fact that the thicknesses *a* and *b* vary considerably (in a nonsystematic way) as the droplet volume is increased from 10 to 60 pl. The cause for this variation in *a* and *b* could be due to slight differences in the amount of water vapor adsorbed on the Si wafer for different experiments; the presence of water vapor is known to influence the spreading kinetics in other experiments [22].

In analyzing the ellipsometric images of the droplet we have assumed that the density and refractive index of the drop are constant and equal to their bulk values. The volume of the droplets can be measured to an accuracy of approximately 1%. From data for the larger droplets we estimate that there was a systematic decrease in volume of the order of 0.5% per hour, which is probably due to slow evaporation.

The total spreading time was 1 to 4 hours so that the effects due to evaporation are small.

We have checked that the hole in the second terrace still forms (i) at 60 °C and (ii) in an environment of higher liquid crystal vapor pressure at 55 °C. The dynamics in both of these situations was similar to the results reported in this publication. This suggests that the appearance of the hole is not related to the proximity to the melting point or to the presence of slow evaporation.

IV. MODEL OF de GENNES AND CAZABAT

The dGC model [7] for terraced droplets describes the evolution of drops structured in terraces of equal thickness assuming that the molecules evolve as a two dimensional incompressible fluid in each terrace where the fluid permeates from the upper terrace to the lower terrace only in a thin annulus at the borders of each terrace. This model does not explain why the droplets are terraced, but allows the computation of the time evolution of the radius of each terrace. Here we adapt this model for droplets possessing two terraces of differing thickness. Most of these formulas are derived in Ref. [7], but we shall include them here for clarity. In the following section we extend the dGC model by incorporating a hole at the center of the second terrace. For those readers whose main interest is in a comparison between the extended dGC model and experiment the remainder of this paper has been written so that the theory in Secs. IV–VI can be omitted without a significant loss in understanding of Sec. VII where this comparison is made.

In the dGC model we assume that the first terrace has a thickness a and the second terrace has a thickness b (Fig. 1). The three main assumptions of this model are as follows.

(a) In the zones where there are two terraces, the fluid descends by permeation from the second terrace to the first with a flux (volume/area/time) given by

$$J_z(r)=C[\mu_1(r)-\mu_2(r)]. \tag{1}$$

The flow is downward when the flux J_z is negative. $C>0$ is the permeation constant [23], $\mu_1(r)$ and $\mu_2(r)$ are the chemical potentials in the first and second terraces, respectively, given by $\mu_i(r)=\mu_0+vp(r)+W_i$. μ_0 is a (irrelevant) reference chemical potential, $p(r)$ is the relative pressure with respect to the atmospheric pressure, v is the molecular volume, and W_i represent the interaction of a molecule in terrace i with the solid substrate. $W_1=-S_0\Sigma$ where S_0 is the monolayer spreading coefficient and Σ is the area per molecule while, for nonretarded dispersion interactions, $W_2\sim -Av/(a+b)^3$ where A is the Hamaker constant. For spreading across the substrate we require that both W_1 and W_2 are negative with $|W_1|>|W_2|$. At the terrace borders, the relative pressure is zero and thus, the potentials are $\mu_i=W_i$.

(b) The molecules move along each terrace according to the equation for incompressible flow. Therefore, the mass conservation equation for two-dimensional flow in each terrace is given by

$$a\ \mathrm{div}\, V_1=-J_z, \tag{2}$$

$$b\ \mathrm{div}\, V_2=J_z, \tag{3}$$

where V_i is the horizontal velocity along terrace i and $\mathrm{div}\, V=1/r\,\partial(rV)/\partial r$ represents the divergence operator for radial symmetry. In the sections of the drop where only the first terrace exists, namely, for $r>R_2$, we have simply $\mathrm{div}V_1=0$.

(c) The velocities and the chemical potentials are related by the simple linear relationships

$$-\nabla\mu_1=\zeta_1 V_1+\zeta(V_1-V_2), \tag{4}$$

$$-\nabla\mu_2=\zeta(V_2-V_1), \tag{5}$$

where ζ_1 and ζ are the friction coefficients between the first terrace and the substrate and between the two terraces, respectively. If the flow in the second terrace can be described by the equations for a viscous fluid then $\zeta=\eta v/b^2$, where η is the macroscopic viscosity of the fluid. In general, the value of ζ_1 will depend upon the details of the fluid-solid interaction.

If we take the difference between Eqs. (4) and (5) and apply the divergence to both sides then using Eqs. (1)–(3), we obtain the differential equation

$$\nabla^2(\mu_1-\mu_2)=\frac{\mu_1-\mu_2}{\xi^2}, \tag{6}$$

where the permeation length is

$$\xi=[C(2\zeta(1/a+1/b)+\zeta_1/a)]^{-1/2}. \tag{7}$$

This is the characteristic length scale over which permeation occurs between the terraces.

Following dGC, we restrict ourselves to cases where the permeation is concentrated in a narrow region of the order of ξ near the border at R_2, with

$$\xi\ll R_2. \tag{8}$$

Thus, in this region $\nabla^2\approx d^2/dr^2$, and from Eq. (6),

$$\mu_2-\mu_1\simeq\Delta\exp[(r-R_2)/\xi], \tag{9}$$

where Δ is a constant that determines the difference in chemical potentials between the second and the first terrace at $r=R_2$. An expression for Δ will be determined later in this calculation. We have $\mu_1=\mu_2$ if $r<R_2-L$; here L is the size of the permeation annulus (Fig. 1) and

$$\xi\ll L\ll R_2, \tag{10}$$

where, for example, $L\sim 5\xi$.

The horizontal velocities within the permeation region for each terrace can now be determined by integrating Eqs. (2) and (3) and computing the flux from Eqs. (1) and (9),

$$V_1=\frac{C}{a}\xi\Delta\exp[(r-R_2)/\xi], \tag{11}$$

$$V_2=-\frac{C}{b}\xi\Delta\exp[(r-R_2)/\xi], \tag{12}$$

where r is restricted to the region $R_2-L<r\leqslant R_2$. We have assumed that the velocities at R_2-L are negligible.

Within the region $R_2<r<R_1$ only one layer is present, consequently there is no permeation and $\mathrm{div}V_1=0$ [Eq. (2)], $-\nabla\mu_1=\zeta_1 V_1$ [Eq. (4)], and therefore $\nabla^2\mu_1=0$. Thus, in this region,

$$\mu_1=(W_2-W_1-\Delta)\frac{\ln(R_1/r)}{\ln(R_1/R_2)}+W_1, \tag{13}$$

where this equation satisfies the boundary conditions $\mu_1(R_1)=W_1$ and $\mu_1(R_2)=W_2-\Delta$ [see Eq. (9)]. The corresponding velocity field is

$$V_1=-\nabla\mu_1/\zeta_1=\frac{W_2-W_1-\Delta}{\zeta_1 r\ln(R_1/R_2)}. \tag{14}$$

Now we can determine a value for Δ by matching the velocities at $r=R_2$ using Eqs. (11) and (14). We obtain

$$\Delta=\frac{W_2-W_1}{C\xi\zeta_1 R_2\ln(R_1/R_2)/a+1}\sim O(\xi/R_2), \tag{15}$$

where the order of the approximation for Δ was estimated using Eq. (7). It is interesting to note that Δ is positive and therefore according to Eqs. (1) and (9) the vertical flux is negative corresponding to a downward flow as one would expect for spreading droplets.

Finally, the velocity at the border of the first terrace is equal to the growth of the radius R_1, therefore,

$$R_1\frac{dR_1}{dt}=\frac{W_2-W_1-\Delta}{\zeta_1\ln(R_1/R_2)} \tag{16}$$

from Eq. (14). The evolution of the second terrace may be obtained from Eq. (16) together with the conservation of volume $V=\pi aR_1^2+\pi bR_2^2=\mathrm{const}$. More details about this model can be found in Ref. [7].

V. GROWTH OF THE HOLE

Now we shall demonstrate that the above solution is unstable with respect to the appearance of a hole at the center of the second terrace. Let us assume that a small hole of radius R_3 is initially created (by some agent not included in this model) at the center of the droplet (Fig. 1), where the thickness inside the hole is a and the velocity V_1 must be zero since the first layer has constant thickness. At the border R_3 of this hole, the chemical potential will be $\mu_2=W_2$. However, as we will demonstrate, the permeation in the neighborhood of R_2 creates a local drop in the chemical potential (Fig. 4) and as a consequence of this gradient in chemical potential, fluid flow will occur in the second terrace between R_3 and R_2.

In order to compute the drop in the potential due to the permeation near R_2, we integrate Eq. (5) using the expressions for the velocities given in Eqs. (11) and (12). We find that at a small distance L from the border of the second terrace

$$\mu_2(R_2-L)=\mu_2(R_2)-\Delta_p, \tag{17}$$

where

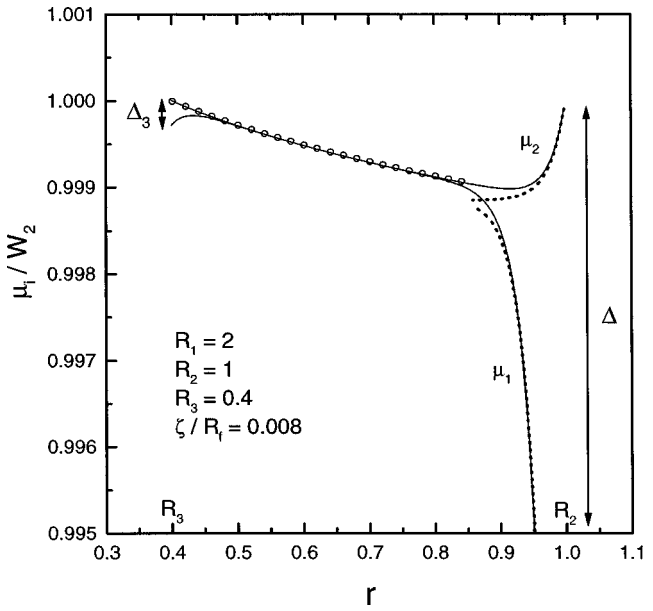

FIG. 4. Comparison of the chemical potentials, μ_1 and μ_2, assumed in Secs. IV and V in the region $R_3<r<R_2$ with an exact numerical solution determined in the Appendix. In Sec. V we assume that $\mu_1\approx\mu_2$ for $R_3<r<R_2-L$, where $L\sim 5\xi$; the logarithmic approximation for $\mu_2(r)$ [Eq. (20)] in this region is shown as open circles. The exact numerical solutions of Eqs. (A1) and (A2) for μ_1 and μ_2 are shown as solid lines. At $R_2=1$ and $R_3=0.4$ the chemical potential difference $\mu_2-\mu_1$ is described, respectively, by the terms Δ and Δ_3. The large difference between Δ and Δ_3 shown in this figure indicates that the permeation at R_2 is much greater than the permeation at R_3 [Eq. (19)]. We also show the approximate exponential solutions for μ_1 and μ_2 (dotted lines) in the region $R_2-L<r<R_2$ determined from Eqs. (4), (5), (11), and (12).

$$\Delta_p=\zeta C\Delta\xi^2(1/a+1/b)\sim O(\xi/R_2). \tag{18}$$

Here we have assumed that the velocities at $r<R_2-L$ are very small compared with the velocities in the vicinity of R_2. In determining the order of the approximation for Δ_p we have used Eqs. (7) and (15). Permeation also occurs at R_3 but, as we will show later, it is much smaller than the permeation at R_2. In fact,

$$J_z(R_3)\sim(\xi/R_3)J_z(R_2). \tag{19}$$

The flow in the region $R_3<r<R_2-L$ is approximately governed by $\nabla^2\mu_2\approx 0$ since $\mu_1\approx\mu_2$ in this region (because the permeation is negligible). This condition for μ_2 can be deduced from Eqs. (1)–(3) and (5). Therefore, the chemical potential must have the form

$$\mu_2=-\Delta_p\frac{\ln(r/R_3)}{\ln[(R_2-L)/R_3]}+W_2, \tag{20}$$

which satisfies Eq. (17) and $\mu_2(R_3)\approx W_2$.

Within the second terrace at a distance much greater than ξ from the borders $\mu_1\approx\mu_2$ and, therefore, from Eqs. (4) and (5),

$$V_2(r)=\frac{\zeta_1+2\zeta}{2\zeta}V_1(r). \tag{21}$$

The corresponding velocity field in this region is given by

$$V_2 \approx \frac{2\zeta+\zeta_1}{\zeta}\frac{\Delta_p}{\zeta_1}\frac{1}{r\ln(R_2/R_3)}, \tag{22}$$

where we have used Eqs. (5), (20), and (21) to obtain this result.

All the mass that comes from the hole is transported by the flow in the two terraces, therefore

$$2\pi b R_3 \frac{dR_3}{dt} = 2\pi a R_3 V_1(R_3) + 2\pi b R_3 V_2(R_3), \tag{23}$$

and using Eqs. (21) and (22) we obtain a differential equation that describes the growth of the hole

$$R_3\frac{dR_3}{dt} \approx \left(\frac{a}{b}+\frac{\zeta_1+2\zeta}{2\zeta}\right)\frac{2\Delta_p}{\zeta_1\ln(R_2/R_3)}, \tag{24}$$

where Δ_p is given in Eq. (18).

In order to obtain the time evolution of a drop, we must integrate this equation together with the conservation of mass

$$V = \pi a R_1^2 + \pi b(R_2^2 - R_3^2) = \text{const} \tag{25}$$

and the equation for the outer terrace, Eq. (16). Corrections to Eq. (16) due to the permeation at R_3 are only of order ξ^2/R_2R_3 and can therefore be neglected.

These evolution equations which describe the spreading dynamics of a two-terraced droplet, Eqs. (16), (24), and (25), can conveniently be written in terms of a dimensionless radius $r_i = R_i/R_f$ and a dimensionless time $\tau = t/t_c$ where the characteristic time is $t_c = R_f^2\zeta_1/(W_2 - W_1)$:

$$r_1\frac{dr_1}{d\tau} = \frac{1}{\ln(r_1/r_2)}\left(1-\frac{\Delta}{W_2-W_1}\right), \tag{26}$$

$$r_3\frac{dr_3}{d\tau} = \frac{2(a/b+\zeta_1/2\zeta+1)}{\ln(r_2/r_3)}\frac{(1+a/b)(\zeta/\zeta_1)}{(2\zeta/\zeta_1)(1+a/b)+1}\frac{\Delta}{W_2-W_1}, \tag{27}$$

the dimensionless potential drop is given by

$$\frac{\Delta}{W_2-W_1} = \frac{1}{(R_f/\xi)r_2\ln(r_1/r_2)/[1+2\zeta/\zeta_1(1+a/b)]+1}, \tag{28}$$

and the dimensionless conservation of mass is now

$$r_1^2 + (r_2^2 - r_3^2)b/a = 1. \tag{29}$$

Equations (26)–(29) can readily be solved numerically by standard methods, for instance, using a Runge-Kutta scheme [25]. At $\tau = 0$, the initial condition is $r_1 = r_2 = \sqrt{a/(a+b)}$ from Eq. (29) with $r_3 = 0$.

VI. RANGE OF VALIDITY FOR THE EXTENDED dGC MODEL

According to our approximations thus far Eqs. (11) and (12) will continue to describe the velocity flow in the immediate vicinity of R_2 provided that the absolute magnitude of the velocity V_2 at R_2 calculated from Eq. (12) is much greater than the velocity field determined from Eq. (22) also evaluated at R_2. This condition may be written as

$$\xi/R_2 \ll \frac{\zeta_1}{2\zeta+\zeta_1}\frac{1}{b/a+1}\ln(R_2/R_3). \tag{30}$$

In this publication we assume small permeation lengths ξ compared with R_i and therefore the approximation (30) is valid provided that we are not too close to the completion time for spreading where $R_2 \approx R_3$. If Eq. (30) is well satisfied then our analytic expressions for μ_i are very accurate. In Fig. 4 we compare Eq. (20) for μ_2 in the region $R_3 < r < R_2 - L$ (open circles) with an exact numerical solution of the equations for μ_1 and μ_2 (solid lines) given in the Appendix for a specific set of values for R_1, R_2, and R_3. In the same figure we also show our solutions for μ_1 and μ_2 (dotted lines) in the region $R_2 - L < r \leqslant R_2$ determined from Eqs. (4), (5), (11), and (12). The analytic expressions agree with the exact numerical solutions extremely well in the bulk of the drop, where the logarithmic approximation holds Eq. (20), and in the vicinity of R_2; these are the two regimes which primarly determine the flow behavior of the drop.

In Sec. V we also assumed that μ_2 is approximately equal to W_2 in the vicinity of R_3 [Eq. (20)]. This is a reasonable assumption because the potential difference at a small distance ξ from the border R_3 is of the order of $\Delta\mu \sim V_2(R_3)\zeta\xi$ according to Eqs. (5) and (21); this quantity is of order $\Delta_p\xi/R_3\ln(R_2/R_3) \sim O(\xi^2/R_2R_3)$ using Eq. (22), and thus, negligible with respect to Δ_p. This means that in the neighborhood of R_3 there is permeation, but it does not significantly affect the chemical potential.

We are now in a position to compare the permeation at R_3 to the permeation at R_2. The permeation flux near R_3 is given by

$$Q_3 = \int_{R_3}^{R_3+\xi} J_z(r)\,2\pi r\,dr \approx 2\pi R_3 C\Delta_3\xi, \tag{31}$$

where we have used the equation for the vertical flux at position r,

$$J_z(r) = C[\mu_1(r) - \mu_2(r)] = C\Delta_3\exp[(R_3 - r)/\xi], \tag{32}$$

and Δ_3 represents the chemical potential difference between the first and second terrace at R_3. [Equation (32) is analogous to Eqs. (1) and (9) applied at R_3.] This permeation flux creates a velocity field V_1 in the first terrace,

$$2\pi R_3 C\Delta_3\xi = 2\pi R_3 a V_1(R_3). \tag{33}$$

Therefore, the difference between the potentials in the two terraces is $\Delta_3 = V_1(R_3)a/C\xi$, and, by using Eqs. (18), (21), and (22), we find that

$$\Delta_3 \sim \Delta\xi/R_3\ln(R_2/R_3). \tag{34}$$

This equation corresponds precisely to the statement given in Eq. (19) [using Eqs. (1), (9), and (32)].

VII. ANALYSIS AND COMPARISON WITH EXPERIMENT

In Secs. IV and V we have derived equations [(16), (24), and (25)] which completely describe the dynamics of a two-terraced droplet possessing a hole at the center of the second terrace (Fig. 1). Dimensionless forms for these equations are also given in Eqs. (26)–(29). These equations are valid provided that the inequality given in Eq. (30) holds. This inequality corresponds approximately to the condition that the permeation length $\xi \ll R_2 - R_3$, so the equations become invalid near the spreading completion time when $R_2 \approx R_3$. From Eqs. (26)–(29) the evolution dynamics are completely determined by the dimensionless ratios ξ/R_f, ζ_1/ζ, and b/a. As noted by dGC, the evolution of the dimensionless radius r_1 [Eq. (26)] is relatively insensitive to the permeation dynamics because the dimensionless potential drop $\Delta/(W_2 - W_1)$, Eq. (28), is proportional to ξ/R_f which is assumed to be much smaller than one. However, the growth of the hole [Eq. (27)], represented by the dimensionless radius r_3, is directly proportional to $\Delta/(W_2 - W_1)$ and therefore extremely sensitive to the permeation dynamics.

In order to be able to compute the solution of these evolution equations, we will assume that each terrace acts as a viscous fluid, so that $\zeta_1/\zeta = (b/a)^2$. This assumption is expected to be a valid approximation for the second terrace [7], namely, $\zeta = \eta v/b^2$, while for the first terrace Fraysse *et al.* [10] have essentially demonstrated that $(W_2 - W_1)/\zeta_1$ is proportional to $1/\eta$, where η is the bulk viscosity and therefore from dimensional considerations we expect that $\zeta_1 \approx \eta v/a^2$. Helfrich [23] has used a similar relationship for the friction coefficient to describe the unusual flow behavior of smectic liquid crystals in small capillaries.

In order to examine the sensitivity of the curves to changes in the permeation length we have plotted r_i as a function of the normalized time $T = \tau/\tau_l$ (Fig. 5) where $\tau_l \approx 0.44$ is the dimensionless time when the second terrace disappears. In this calculation we have set $b/a = 5.5$ (the average experimental value) and varied ξ/R_f; the dotted and dashed lines correspond, respectively, to $\xi/R_f = 0.001$ and 0.01. As expected r_1 is not very sensitive to this parameter while r_3 depends sensitively upon ξ/R_f. The cusp in r_2 and r_3 near $T = 1$ is caused by the failure of Eq. (30) when our analytic approximations are no longer valid. In this figure we have also plotted the curves for $b/a = 3.0$ and $\xi/R_f = 0.001$ (solid lines) where in this calculation the dimensionless lifetime $\tau_l = 0.34$. One observes from the two curves where $\xi/R_f = 0.001$ (solid and dotted lines) that the magnitude of r_3 and the behavior in the region where $r_2 \approx r_3$ (near the completion time at $T = 1$) are relatively insensitive to the value of b/a.

We now compare the extended dGC theory with experiments. In Fig. 3(b) we have plotted the averaged normalized radius $r_i = R_i/R_f$ as a function of the normalized time $T = (t - t_0)/t_l$ for three different droplets with volumes varying from 9 to 60 pl (symbols). As defined above, $t_l = t_f - t_0$ is the spreading lifetime when the second terrace disappears and the spreading stops. Our model is strictly valid only when a and b are time independent, which according to Fig. 3(a) occurs when $T > 0.2$. We have fixed $b/a = 5.5$, the experimental average value, and allowed ξ/R_f to vary in order to find the best fit to the experiments (solid lines), which occurs

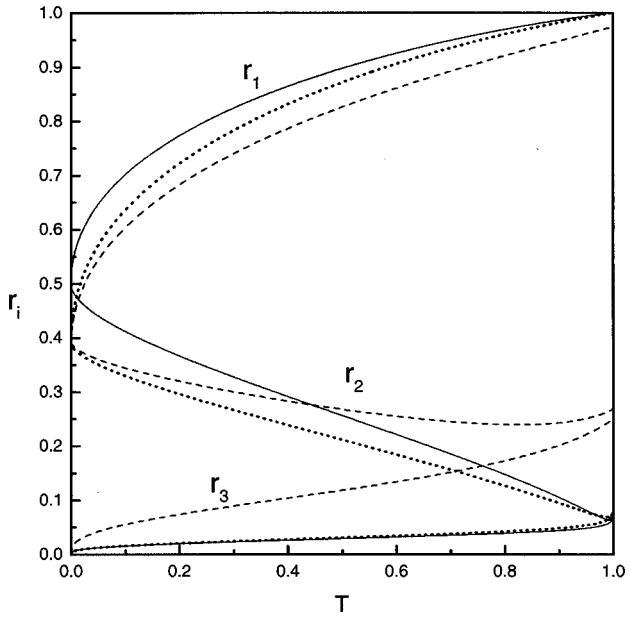

FIG. 5. Theoretical evolution curves determined from Eqs. (26)–(29) for $b/a = 5.5$ (the experimental average) and $\xi/R_f = 0.001$ (dotted lines) and 0.01 (dashed lines). We also show the influence of varying the quantity b/a; the solid lines are for $b/a = 3.0$ and $\xi/R_f = 0.001$.

for $\xi/R_f = 0.0025$. From this value for ξ/R_f we determine the permeation length ξ for each droplet. The average permeation length of approximately 3 μm is consistent with the experimental observation that the step edge between the first and second terraces at R_2 is sharper than our experimental resolution of ~ 10 μm. If the permeation length ξ happened to exceed our experimental resolution we would expect to observe rounding at the border between the two terraces. Table I exhibits a considerable variation between the permeation lengths for different droplets. The thickness a of the first terrace also shows a large variation between droplets which could be indicative of differing molecular properties within the terrace, which according to Ref. [24] could give rise to different values for ξ.

Following Ref. [10], from Eq. (26) with $\Delta/(W_2 - W_1) \ll 1$, we determine that the quantity $R_1 \ln(R_1/R_2) dR_1/dt$ is approximately independent of time; this quantity provides a value for the ''diffusion coefficient'' $D = (W_2 - W_1)/\zeta_1 = (1.6 \pm 0.3) \times 10^{-6}$ cm^2/s for the three droplets (Fig. 6 and Table I). The dimensionless terrace lifetime calculated from $\tau_l(\text{expt}) = t_l/t_c = (t_f - t_0)(W_2 - W_1)/\zeta_1 R_f^2 = 0.5 \pm 0.1$, and given in Table I for the three drops, agrees within experimental errors with the numerically determined dimensionless lifetime of $\tau_l = 0.44$ for $b/a = 5.5$.

The agreement between theory and experiment is only

TABLE I. Experimental droplet parameters.

V (pl)	a (Å)	b/a	$t_1 = t_f - t_0$ (s)	ξ (μm)	D (cm 2/s)	τ_1 (expt)
9.15	34.3	5.44	3980	2.3	1.26×10^{-6}	0.59
24.4	45.2	7.86	3740	3.3	1.70×10^{-6}	0.37
60.5	40.6	3.19	15 400	5.4	1.79×10^{-6}	0.58

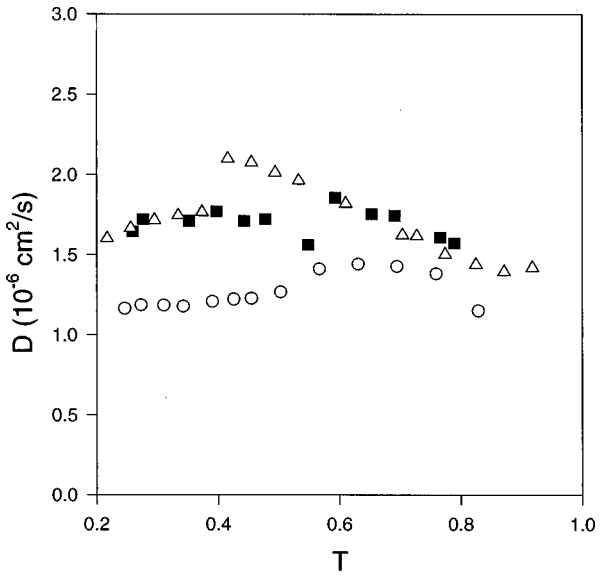

FIG. 6. Plot of the ''diffusion coefficient'' $D=R_1\ln(R_1/R_2)dR_1/dt$ versus normalized time T for the three droplets: 9.1 pl (circles), 24.4 pl (squares), and 60.5 pl (triangles).

qualitative [Fig. (3)]; approximate agreement is obtained for the shape of the reduced radii curves r_i as a function of the normalized time T. The experimental data exhibits a greater universality in form which is much less sensitive to the values of b/a and ξ/R_f than theory would indicate. We do not believe that the discrepancies between theory and experiment are caused by our assumption that $\zeta_1/\zeta=(b/a)^2$. We have also considered other limiting cases, such as $\zeta_1/\zeta\gg 1$ and $\zeta_1/\zeta\ll 1$; the parameter ζ_1/ζ cannot improve the agreement between theory and experiment. We believe that part of the problem may be due to the irregular inner and outer borders of the second terrace [Fig. 2(b)]; R_2 and R_3 only represent the average radii for these borders. These irregularities are not included within the theory; they indicate that the velocity flows at the borders of the second terrace, at any instance in time, are far more complicated than described by Eqs. (11), (12), and (24).

VIII. SUMMARY

In this paper we have studied the spreading dynamics of microdroplets ($9-60$ pl) of the liquid crystal $\overline{7}S5$ on a molecularly flat, uv-ozone cleaned (100) Si wafer possessing a ~ 20 Å thick silicon oxide layer at a temperature of $\sim 1.5\,^{\circ}$C above the liquid crystal melting point. At early times this liquid crystal droplet possesses a rounded shape, as in capillary dominated spreading, but with a sharp border where the liquid crystal height decreases suddenly over ~ 250 Å to the the wafer value. With increasing time the droplet evolves into two terraces where the lower terrace possesses a thickness of ~ 40 Å while the upper terrace possesses a thickness of ~ 200 Å [Fig. 2(a)]. Both terraces are extremely flat on top and the step edge between the two terraces is sharper than our horizontal spatial resolution of ~ 10 μm. This system constitutes the simplest system with which to test the predictions of the de Gennes and Cazabat model [7] for terraced spreading. Surprisingly we have discovered that a hole develops in the upper terrace soon after this terrace acquires a flat top. This hole propagates down to the depth of the first terrace. We have extended the de Gennes and Cazabat model to include a hole in the upper terrace. The resulting dimensionless analytic expressions for the spreading dynamics of two-terraced droplets, possessing a hole in the upper terrace, are given in Eqs. (26)–(29); these expressions are expected to remain valid provided that the inequality in Eq. (30) holds, namely, for small permeation lengths compared with the outer radius of the upper terrace (R_2) and provided that the spreading is not too near the spreading lifetime when $R_2\approx R_3$. According to Eq. (27) a hole must form in the second terrace for spreading droplets which obey the rules set out by de Gennes and Cazabat [7] because the growth velocity of the hole $dr_3/d\tau \sim 1/r_3\ln(r_2/r_3)$ is positive and diverges for small r_3 (the dimensionless radius of the hole), namely, any small perturbations are unstable and must grow. We have found that the dimensionless equations provide a good description of the average spreading dynamics where $b/a=5.5$ [Fig. 3(b)] for a permeation length of $\xi\sim 3$ μm. From the value of $R_1\ln(R_1/R_2)dR_1/dt$ we determined the average diffusion coefficient for the first terrace $(W_2-W_1)/\zeta_1\approx 1.6\times 10^{-6}$ cm^2/s. This quantity is expected to depend mainly upon the interaction of the liquid crystal with the Si wafer surface.

One may conclude that the theory appears to provide a good description of the average evolution of two-terraced droplets possessing flat terraces and sharp boundaries between the first and the second terrace. It provides an explanation of why the hole must develop in the second terrace. However, the theory omits important features which are observed experimental, such as, the irregularities of the second terrace at late times. It would be very useful if the permeation length (~ 3 μm) could be determined directly via experiment. This can perhaps now be accomplished using an atomic force microscope [26].

ACKNOWLEDGMENTS

This research work has been supported by the National Science Foundation through Grant Nos. DMR-9631133 (B.M.L.) and DMR-9703898 (C.C.H.).

APPENDIX

In Sec. V we derived an approximate analytic expression for μ_2 [Eq. (20)] in the region $R_3<r<R_2-L$ where $L\approx 5\xi$. This equation is expected to be valid for small ξ/R_2 according to condition (30). In order to check this approximation we solve numerically the corresponding coupled differential equations in this appendix, without making the assumption that $\xi/R_2\ll 1$. Equations (1)–(5) can be reformulated as

$$\nabla^2\mu_2=C\zeta(1/a+1/b)[2\mu_2-(\mu_1+\mu_2)] \qquad \text{(A1)}$$

and

$$\nabla^2(\mu_1+\mu_2)=(C\zeta_1/a)[(\mu_1+\mu_2)-2\mu_2]. \qquad \text{(A2)}$$

The boundary conditions for these equations at R_3 are $\mu_2=W_2$ and $d/dr(\mu_1+\mu_2)=0$ where the second condition

comes from Eqs. (4) and (5) with $V_1=0$ at R_3. At R_2 the boundary conditions are $\mu_2=W_2$ and $(\mu_1+\mu_2)-W_1-\mu_2=-R_2\ln(R_1/R_2)d(\mu_1+\mu_2)/dr$. The later boundary condition represents the velocity continuity in the first terrace, and comes from Eqs. (4), (5), and (14) with $\Delta=\mu_2-\mu_1$ at R_2. These coupled equations are solved numerically using a Runge-Kutta scheme, and the boundary conditions are adjusted by the shooting method [25].

In Fig. 4 we compare a numerical solution (solid lines) to Eqs. (A1) and (A2) for $R_1=2$, $R_2=1$, $R_3=0.4$, and $\xi/R_f=0.008$ with the asymptotic logarithmic approximation for μ_2 (open circles) given in Eq. (20) which is valid in the region $R_3<r<R_2-5\xi$. We also compare the approximate exponential expressions for μ_1 and μ_2 (dotted lines) in the region $R_2-5\xi<r<R_2$ derived from Eqs. (4), (5), (11), and (12). We observe good agreement between the approximations and the exact numerical solution. The potential difference $\mu_2-\mu_1$ at $r=R_2$ in this figure is much larger than the corresponding difference at $r=R_3$; this is indicative that the permeation at R_2 is much greater than the permeation at R_3.

[1] P. G. de Gennes, Rev. Mod. Phys. **57**, 827 (1985).

[2] A. W. Adamson, *Physical Chemistry of Surfaces*, 4th ed. (Wiley, New York, 1982).

[3] W. B. Hardy, Philos. Mag. **38**, 49 (1919).

[4] D. Ausserré, A. M. Picard, and L. Léger, Phys. Rev. Lett. **57**, 2671 (1986); L. Léger, M. Erman, A. M. Guinet-Picard, D. Ausserré, and C. Strazielle, *ibid.* **60**, 2390 (1988); D. Beaglehole, J. Phys. Chem. **93**, 893 (1989).

[5] F. Heslot, N. Fraysse, and A. M. Cazabat, Nature (London) **338**, 640 (1989); F. Heslot, A. M. Cazabat, and P. Levinson, Phys. Rev. Lett. **62**, 1286 (1989).

[6] A. M. Cazabat, N. Fraysse, F. Heslot, P. Levinson, J. Marsh, F. Tiberg, and M. P. Valignat, Adv. Colloid Interface Sci. **48**, 1 (1994); S. Bardon, M. Cachile, A. M. Cazabat, X. Fanton, M. P. Valignat, and S. Villette, Faraday Discuss. **104**, 307 (1996).

[7] P. G. de Gennes and A. M. Cazabat, C. R. Acad. Sci., Ser. II: Mec. Phys., Chim., Sci. Terre Univers **310**, 1601 (1990).

[8] D. B. Abraham, P. Collet, J. De Coninck, and F. Dunlop, Phys. Rev. Lett. **65**, 195 (1990); S. F. Burlatsky, G. Oshanin, A. M. Cazabat, and M. Moreau, *ibid.* **76**, 86 (1996).

[9] J. Yang, J. Koplik, and J. R. Banavar, Phys. Rev. Lett. **67**, 3539 (1991); J. De Coninck, N. Fraysse, M. P. Valignat, and A. M. Cazabat, Langmuir **9**, 1906 (1993); J. DeConinck, U. D'Ortona, J. Koplik, and J. R. Banavar, Phys. Rev. Lett. **74**, 928 (1995); S. Bekink, S. Karaborni, G. Verbist, and K. Esselink, *ibid.* **76**, 3766 (1996).

[10] N. Fraysse, M. P. Valignat, A. M. Cazabat, F. Heslot, and P. Levinson, Adv. Colloid Interface Sci. **158**, 27 (1993).

[11] M. P. Valignat, N. Fraysse, A. M. Cazabat, P. Levinson, F. Heslot, and M. Cazabat, Colloids Surf., A **83**, 193 (1994).

[12] J. Daillant, G. Zalczer, and J. J. Benattar, Phys. Rev. A **46**, R6158 (1992).

[13] W. Kern and D. A. Puotinen, RCA Rev. **31**, 187 (1970).

[14] L. Holland, *The Properties of Glass Surfaces* (Chapman and Hall, London, 1964).

[15] J. Vig, J. Vac. Sci. Technol. A **3**, 1027 (1985).

[16] J. Chrusciel, L. Richter, and M. Rachwalska, Mol. Cryst. Liq. Cryst. **75**, 155 (1981).

[17] B. M. Law and H. K. Pak, J. Opt. Soc. Am. A **13**, 379 (1996).

[18] H. K. Pak and B. M. Law, Rev. Sci. Instrum. **66**, 4972 (1995).

[19] R. M. Azzam and N. M. Bashara, *Ellipsometry and Polarized Light* (North-Holland, Amsterdam, 1977).

[20] T. E. Lockhart, E. Geterinter, and M. E. Neubert, Phys. Rev. A **25**, 2262 (1982).

[21] The approximate length of the $\overline{7}S5$ molecule is ~ 28 Å [C. R. Safinya, R. J. Birgeneau, J. D. Litster, and M. E. Neubert, Phys. Rev. Lett. **47**, 668 (1981)], however, we are uncertain as to the average orientation of this molecule on the surface within the first terrace.

[22] S. Villette, M. P. Valignat, A. M. Cazabat, L. Jullien, and F. Tiberg, Langmuir **12**, 825 (1996).

[23] W. Helfrich, Phys. Rev. Lett. **23**, 372 (1969).

[24] D. Ausserrè, F. Brochard-Wyart, and P.-G. de Gennes, C. R. Acad. Sci., Ser. II: Mec. Phys., Chim., Sci. Terre Univers **320**, 131 (1995).

[25] W. H. Press, B. P. Flannery, S. A. Teukolsy, and W. T. Vatterling, *Numerical Recipes* (Cambridge University Press, Cambridge, 1986), pp. 550 and 582.

[26] S. S. Sheiko, A. M. Muzafarov, R. G. Winkler, E. V. Getmanova, G. Eckert, and P. Reineker, Langmuir **13**, 4172 (1997); A. Fery, S. Herminghaus, and D. Reim, Ultramicroscopy **69**, 211 (1997); M. Salmeron, L. Xu, J. Hu, and Q. Dai, Mater. Res. Bull. **22**, 36 (1997).